AIAA SciTech
13-17 January 2014, National Harbor, Maryland
52nd Aerospace Sciences Meeting

Investigation of Non-synchronous Vibration Mechanism for a High Speed Axial Compressor Using Delayed DES

Hong-Sik Im*

Gecheng Zha†
Dept. of Mechanical and Aerospace Engineering, University of Miami
Coral Gables, Florida 33124, USA

Abstract

This paper uses the delayed detached eddy simulation (DDES) of turbulence to investigate the mechanism of non-synchronous vibration (NSV) of a multistage high speed axial compressor. DDES is a hybrid model for turbulence simulation, which uses RANS model within the wall boundary layer and uses large eddy simulation outside of the wall boundary layer. Time accurate Navier-Stokes equations are solved with a 3rd order WENO reconstruction for the inviscid flux and a 2nd order central differencing for the viscous terms. A fully conservative rotor/stator sliding BC is used to resolve the unsteady interaction between the rotor and the stationary blades. A 1/7th annulus sector is employed with the time shifted phase lag BC at the circumferential boundaries. The DDES shows that the NSV of the compressor occurs due to the rotating flow instability in the vicinity of the rotor tip at a stable operation condition. The tornado-like tip vortex causes the NSV of the rotor blades as it propagates to the next blade passage in the counter rotating direction above 80% rotor span. The tornado vortex travels fast on the suction surface of the blade and stays relatively longer at the passage outlet crossing to the next blade leading edge. Such a tornado vortex motion trajectory generates two low pressure regions due to the vortex core positions, one at the leading edge and one at the trailing edge, both are oscillating due to the vortex coming and leaving. These two low pressure regions create a pair of coupling forces that generates a torsion moment causing NSV.

1 Introduction

Non-synchronous vibration of axial fan/compressor is a non-engine order vibration with a large amplitude due to a complex flow phenomenon such as rotating instability (RI) and usually occurs at a stable operating condition[1, 2, 3, 4, 5].

The experiment for the 10 stage high pressure axial compressor by Baumgartner et al.[1] shows a NSV with high amplitude vibration on the 1st stage rotor blades. A rotating flow instability is an instability that revolves relative to the rotor rotation. Measured pressure at various blade span near the rotor leading edge shows the radial dependency of this rotating instability. The measured frequencies give high coherence levels of the NSV above 74% span, which decays away from the rotating instability (RI) and eventually the NSV is no more detectable below 65% blade span. Marz et al.[2] conducted the low speed single stage fan experiment and showed a NSV due to the tip flow instability at around 3000 RPM. The experiment indicates the occurrence of NSV at near the maximum fan loading condition with its frequency at roughly half of blade passing frequency (BPF). The time-lapse plots of casing wall pressure clearly captures a highly fluctuating vortex structure in the rotor entry plane during the NSV event. Another experimental study

* Ph.D., Currently an engineer at Honeywell
† AIAA Associate Fellow, gzha@miami.edu

on axial compressor NSV is carried out by Mailach et al.[3]. Their measurements show that the rotating instability is limited to the blade tip region with its peak amplitude at 92% of the blade height around 20% to 30% of the chord. The strong non-engine order vibration is caused by the fluctuating blade tip vortices that travel in the opposite direction to rotor rotation. These experiments indicate that the propagation of the rotating instability over blade passage causes the NSV.

Numerical simulation of compressor/fan NSV is very important to understand the mechanism and to be used as a design tool. Simulation of turbulent flows is critical for accurate prediction of NSV because the large vortical flow structure plays a key role in the formation of the rotating flow instabilities. The Reynolds-averaged Navier-Strokes (RANS) methods usually cannot predict large flow structures well. Large eddy simulation (LES) is promising to overcome the disadvantages of the RANS model. However, for high Reynolds number flows such as those of turbomachinery blades, LES needs the CPU resource not much less than the Direct Numerical Simulation(DNS) to resolve wall boundary layer.

To overcome the intense CPU requirement for LES, Spalart developed the detached eddy simulation (DES) strategy[6], which is a hybrid RANS and LES method. Near the solid surface within the wall boundary layer, the unsteady RANS model is realized. Away from the wall surface, the model automatically converts to LES. By using the RANS model near walls, the mesh size as well as the CPU time can be tremendously reduced. It is shown[6, 7, 8] that the use of hybrid RANS/LES approaches is very effective for the large structure of vortical flow predictions. In [9], DES is used to simulate the spike stall inception of a transonic rotor.

So far, almost all the NSV simulations are based on RANS model. Kielb et al.[4] conducted the 1/7th annulus sector simulation of the high speed axial compressor rotor using a RANS model. Their simulation shows that the NSV is caused by the suction side vortex oscillation in a blade passage near 75% span. The predicted frequency is underpredicted by roughly 10% compared with the measurement. The full annulus RANS simulation by Marz et al.[2] also shows that the NSV is a local flow instability that does not propagate to the next blade passage. As presented in the section of unsteady 1-1/2 stage NSV DDES simulation, the current simulation clearly captures the travelling vortex instability over the next blade passage during the NSV.

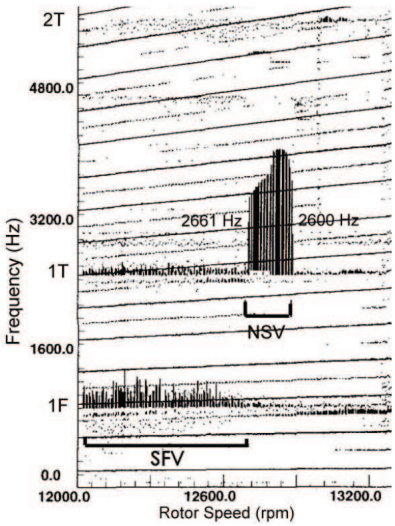

Figure 1: Strain gage response of the first-stage rotor blades of a high-speed compressor showing the frequency lock-in near the 1st torsional mode (1T) during the NSV

The high speed axial compressor adopted in this study exhibits a strong non-engine order vibration of the 1st stage rotor blades close to the blade 1T (1st torsional) mode during the engine test[4], see Fig. 1. The NSV frequency collapses between 2600 Hz and 2661 Hz with a large amplitude, which is considered

as a lock-in phenomenon[10]. Under NSV, no resonance appears but failure of the blade structure such as high cycle fatigue (HCF) can occur. The NSV frequency is shifted from 2600 Hz to 2661 Hz as the rotor speed slightly decreases roughly from 12800 RPM to 12700 RPM. The experiment[4] confirms the NSV occurrence before stall. The rotor tip clearance of the full compressor rig is about 1.1% of tip chord.

In order to reveal the detailed mechanism of NSV, this paper conducts the Delayed Detached Simulation of NSV for a 1-1/2 stage high speed compressor, which has 56 IGVs, 35 rotor blades and 70 stator blades with RPM of 12880.

An accurate shock capturing scheme is necessary to simulate high-speed axial compressors since the rotor blade tips often experience shock/boundary layer interaction. This study uses the Low Diffusion E-CUSP (LDE) Scheme[11] as an accurate shock capturing Riemann solver with a 3rd order WENO reconstruction for inviscid flux and a 2nd order central differencing for viscous terms[12]. An implicit 2nd order dual time stepping method[13] is solved using an unfactored Gauss-Seidel line iteration to achieve high convergence rate. The high-scalability parallel computing is applied to save wall clock time[14].

2 Delayed Detached Eddy Simulation

The unsteady spatially filtered Navier-Stokes equations are solved in a rotating frame[9] with the delayed detached eddy simulation (DDES) of turbulence suggested by the Spalart et al.[15]

DES is based on the S-A one-equation eddy viscosity model[6] to switch between RANS model within wall boundary layer and Subgrid scale stress model of LES outside of boundary layer for large structures. The coefficients c_{t1} and c_{t3} in the S-A model are set to zero and the distance to the nearest wall, d, is replaced by $\tilde{d}$ as

$$\tilde{d} = min(d, C_{DES}\Delta) \tag{1}$$

where Δ is the largest spacing of the grid cell in all the directions. Within the boundary layer close to the wall, $\tilde{d} = d$, hence the turbulence is simulated by RANS mode of Spalart-Allmaras[16]. Away from the boundary layer, $\tilde{d} = C_{DES}\Delta$ is most cases. When the production and destruction terms of the model are balanced, the length scale $\tilde{d}$ will have a Smagorinsky-like eddy viscosity and the turbulence is simulated by the LES model. The coefficient $C_{DES} = 0.65$ is used as set in the homogeneous turbulence[7]. The Pr_t may take the value of 0.9 within the boundary layer for RANS mode and 0.5 for LES mode away from the wall surface.

To overcome the modeled stress depletion problem and make the DES limiter independent of grid spacing, the DDES model suggested by Spalart et al.[15] switches the subgrid scale formulation in S-A model by redefining the distance to the nearest wall $\tilde{d}$ as

$$\tilde{d} = d - f_d max(0, d - C_{DES}\Delta) \tag{2}$$

where

$$f_d = 1 - tanh([8r_d]^3) \tag{3}$$

$$r_d = \frac{\nu_t + \nu}{\sqrt{U_{i,j}}k^2d^2R_e} \tag{4}$$

$$U_{i,j} = \frac{\partial u_i}{\partial x_j}\frac{\partial u_j}{\partial x_i} \tag{5}$$

where Δ is the largest spacing of the grid cell in all the directions, $U_{i,j}$ represents the velocity gradient tensor, and k denotes the Karmann constant. Within the boundary layer close to walls, $\tilde{d} = d$, and away

from the boundary layer, $\tilde{d} = C_{DES}\Delta$ is most of the case. This mechanism enables DDES to behave as a RANS model in the near-wall region, and LES away from walls. This modification in $\tilde{d}$ reduces the grey transition area between RANS and LES.

The validation of current DDES methodology for the stalled flow over NACA0012 airfoil at 45° angle of attack was conducted by the present authors[8]. The DES predicts the drag accurately compared to the experiment, whereas the URANS model overpredicts the drag by about 33%.

3 Boundary Conditions

At the IGV inlet, the radial distributions of total pressure, total temperature, swirl angle and pitch angle are specified and velocity is extrapolated from the computational domain in order to determine the rest of the variables. On the blade surface and casing wall a non-slip boundary condition is applied, while on the hub surface the law of the wall is used to avoid an excessive fine mesh in the boundary layer[9]. At the stator outlet, the static pressure is specified in the spanwise direction. The velocity components are extrapolated from the computational domain and an isentropic relation is used to determine density. If the wall surface is rotating, the wall static pressure for the inviscid momentum equation is determined by solving the radial equilibrium equation. If the wall surface is stationary, the static pressure gradient across the wall boundary is set to zero. In addition, the adiabatic condition is used to impose zero heat flux through the wall.

The fully conservative sliding boundary condition (BC)[17] at the blade row interface is used to resolve wake propagation, shocks interaction and rotating instabilities. In addition, an efficient time-shifted phase-lagged BC[18] with nodal diameter of 5 is applied at the lower/upper circumferential boundaries to facilitate 1/7th annulus simulations.

4 Computational Mesh

The 1/7th sector mesh for 1-1/2 stage of the compressor is presented in Fig. 2. The rotor tip clearance is modeled with 21 grid points using an O-mesh block. The mesh of IGV/rotor/stator is partitioned to total 174 blocks for parallel computation. The mesh around the blade was constructed by using the O-mesh. For the IGV and stator, 121(around blade)×101(blade-to-blade)×71(blade span) is the mesh size, and for the rotor, 201(around blade)×101(blade-to-blade)×71(blade span). H-mesh layer is used for the matched one-to-one grid point connection at the sliding BC interface of IGV/rotor/stator that enables variable exchange in a fully conservative manner. Each H-mesh layer has a mesh size of 201(tangential)×6(aixal)×71(blade span). The total mesh size for this 1/7 sector of 1-1/2 compressor is 12,127,638.

5 Numerical Probes

The numerical probes to acquire the static pressure responses at the tip clearance are shown in Fig. 3. Total 60 points on a blade surface, 5 points in the middle of tip clearance and 5 points at the casing surface are mounted. The first numeral of the probe number means location around blade surface and the second numeral indicates location of blade span. For example, the probe 64 means the 6th probe from the trailing edge and the 4th probe from the hub, which is on the suction surface of 93% blade span near leading edge.

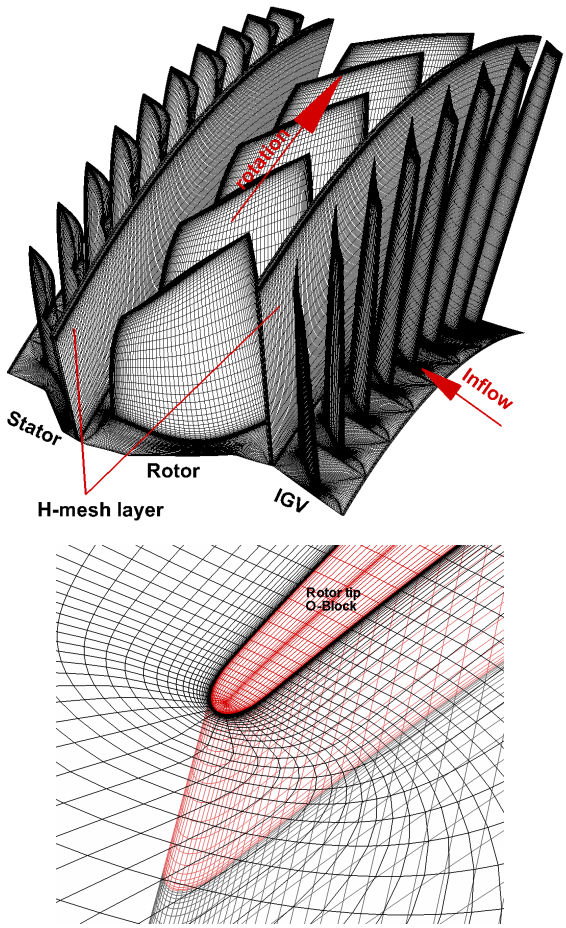

Figure 2: 1/7th Annulus mesh for NSV simulation

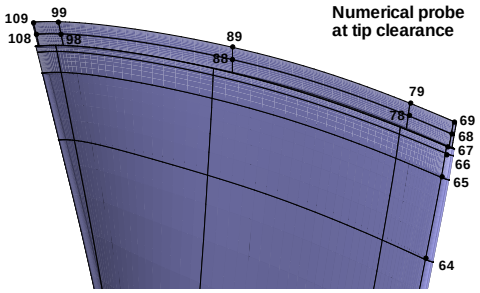

Figure 3: Numerical probes of the rotor blade

6 Unsteady 1-1/2 Stage NSV DDES Simulation

The rig testing of the axial compressor with 1.1% tip clearance[4] is shown to have the NSV frequency range of 2600 Hz to 2661 Hz, which is located between 12EOL(engine order line) to 13EOL as shown in the Campbell diagram in Fig. 4. The measured compressor NSV is at 2600 Hz at the present DDES simulation operating condition of 12880 RPM. The residual is reduced by three orders of magnitude within each physical time step, which is usually achieved within 30 to 40 pseudo time step iterations. A non-dimensional time step of about 0.005 is used. Note the Campbell diagram can be used to evaluate whether a blade frequency including natural frequency is synchronous or not with engine shaft. EOL in Campbell diagram is obtained by integer multiples of rotor shaft frequency with respect to RPM. The NSV predicted

by DDES is 2217 Hz, which is underpredicted by about 14.7% compared to the experiment as shown in Fig. 4.

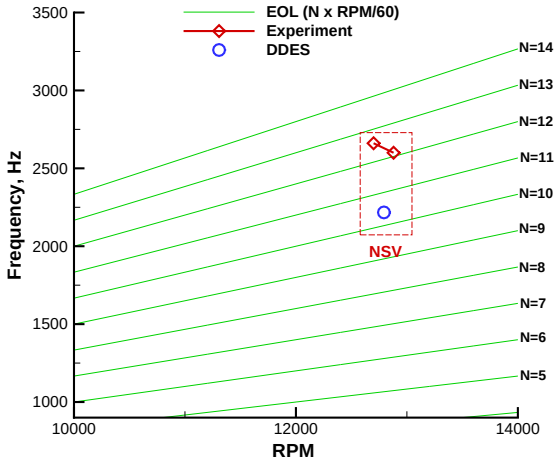

Figure 4: Campbell diagram

6.1 Speedline Characteristics

In Fig. 5, the total pressure ratio of rotor-to-IGV is plotted in terms of the mass flow at RPM of 12880. The thick solid line represents the speedline predicted in [4]. The dashed line indicates possible NSV region obtained by the experiment[4, 5]. The symbol square is the speedline at the NSV of 2365 HZ predicted in [4] by CFD, while the solid circle denotes the NSV of 2217 Hz predicted by present DDES. Difference in the total pressure ratio at NSV between the DDES and the RANS result in [4] is about 0.8% and the mass flow difference between the RANS results of [4] and the DDES is about 4.7%.

Note that NSV of the compressor occurs at a stable operating condition and its frequency varies due to the mass flow, operating speed and temperature[19, 5]. In addition, a URANS for the 1/7th rotor annulus with in-phase condition at the lower/uppper periodic boundaries were used for the NSV simulation in [4]. Therefore, the effects of rotor/stator interaction and phase difference on NSV were neglected by the NSV simulation in [4]. As shown by the earlier work of present authors[5], overall URANS predicts the NSV frequency a little closer to the experiment than the DDES. However, the DDES resolves more details and small structures of the rotating flow instabilities of tornado vortices that cause the NSV as observed in this study.

6.2 Tip Flow Instabilities

The present DDES demonstrates a rotating instability (RI) above 80% rotor span that causes NSV. Fig. 6 shows entropy near the rotor leading edge axial plane. During the NSV of the compressor, entropy above 80% rotor span is significantly increased due to the RI that causes the NSV as it travels circumferentially through the rotor leading edge ahead above 80% span.

As pointed out in the NSV experiment[4, 5], the flow field of the C1 full compressor during the NSV is not developed into a rotating stall where breakdown of the mass flow usually occurs. In the present simulation, the mass flow of the compressor is not decreased like rotating stall as presented in Fig. 7. The mass flow at the rotor outlet oscillates with a phase-locked manner. Since the present DDES simulation is started from the RANS solutions obtained using a mixing plane[17] at the rotor/stator sliding interfaces, it

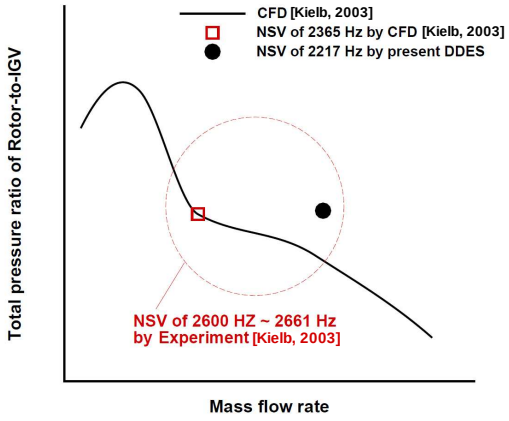

Figure 5: Speedline of the 1-1/2 stage axial compressor predicted by DDES

takes about half rotor revolution for the calculation to reach dynamically stable status as shown in Fig. 7. Note that frequencies presented in this study are obtained based on the instantaneous pressure spectrum over 2 rotor revolutions after the transitional flow disappears.

Fig. 8 shows the instantaneous flow field at the rotor tip section, axial velocity contour (left) and entropy (right). The reversal flow is clearly identified near the 1st stage rotor tip region, which gives rise to significant increase in entropy. The entropy near the upper boundary of the reversal flow has a jump due to the interaction with incoming flow from the IGV.

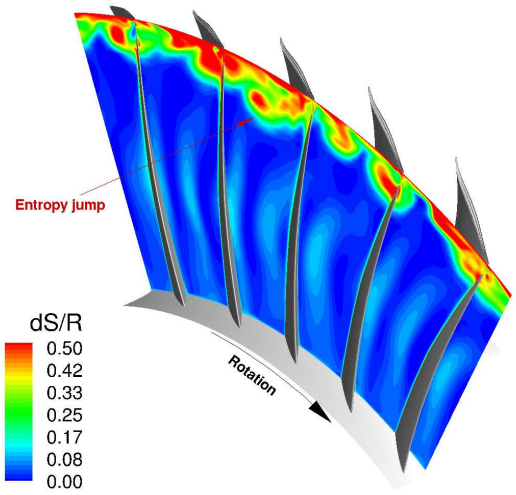

Figure 6: Entropy contour at leading edge axial plane predicted by DDES

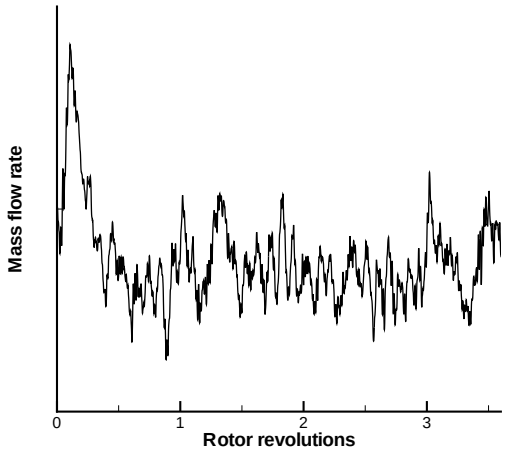

Figure 7: Instantaneous mass flow at the rotor outlet predicted by DDES

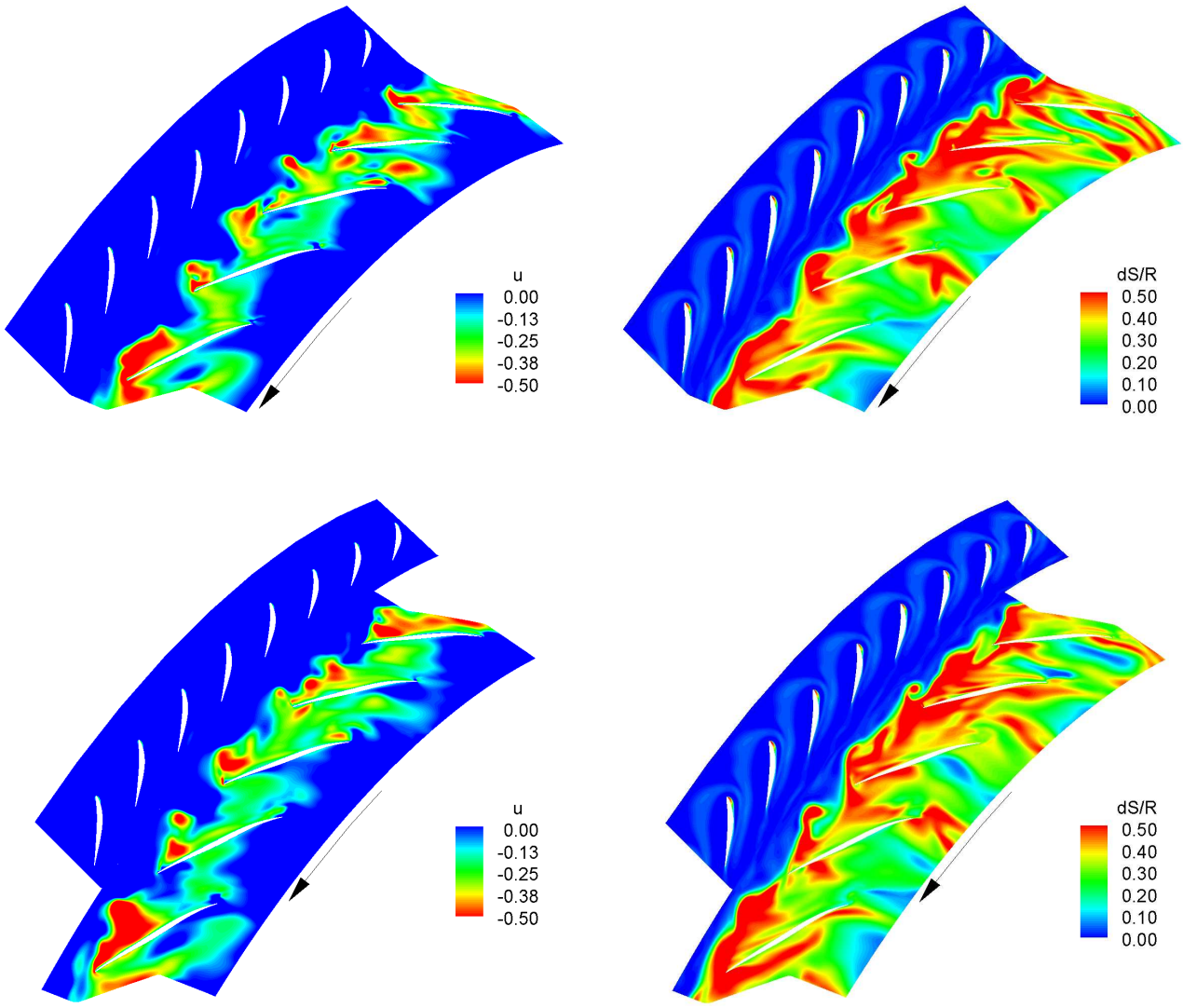

Figure 8: Instantaneous axial velocity contour (left) and entropy (right) at the rotor tip section predicted by DDES; 2 Rev(top), 2+1/35 Rev(bottom)

6.3 Role of Tornado Vortex in NSV

Fig. 9 illustrates the 3D tornado like tip vortex structure as the main cause of the NSV observed in this study. Unlike the regular streamwise tip clearance vortex, it swirls strongly with vortex axis normal to the blade suction surface and induces the reversal flow near the rotor tip region as shown by the color. A similar vortical flow structure is detected by the experimental work of Inoue et al.[20], which is a separation vortex from the blade suction surface and ends up at the casing wall during the short length scale rotating stall of the multistage axial compressor. However, the present DDES demonstrates that the tornado vortex rotates circumferentially through the rotor leading edge ahead roughly above 80% span and causes the NSV of the compressor stage 1 rotor blades.

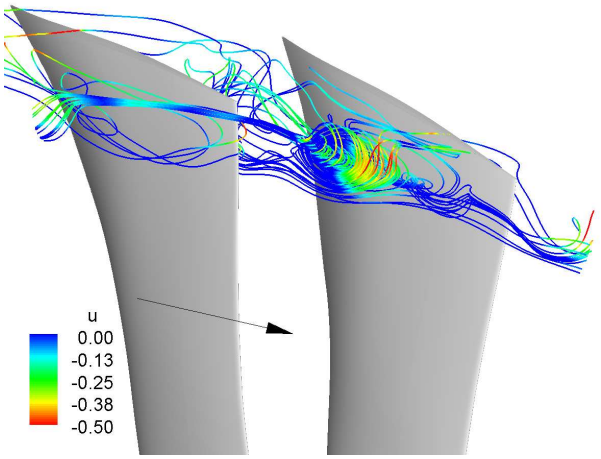

Figure 9: Tornado vortex during the NSV predicted by DDES

Fig. 10 shows the instantaneous tornado vortex movement over 2 rotor blades. The present DDES simulates how the tornado vortex causes the NSV. The tornado vortex on the blade A suction surface at $\frac{1}{35}$ Rev moves to the blade B at $\frac{3}{35}$ Rev in the opposite direction to the rotor rotation. The tornado vortex travels fast on the suction surface of the blade and stays relatively longer at the passage outlet crossing to the next blade leading edge. Such a tornado vortex motion trajectory generates two low pressure regions due to the vortex core positions, one at the leading edge and one at the trailing edge, both are oscillating due to the vortex coming and leaving. These two low pressure regions create a pair of coupling forces that generates a torsion moment causing NSV. This is consistent with the experimental and numerical observations in [4, 18] that the NSV of this rotor is dominant at its first torsion mode(2nd mode). The frequency of this tornado vortex propagation captured is roughly equal to the NSV frequency of the blade pressure signals. Other experiments[3, 1] for axial fan/compressor also show that the flow instabilities in the vicinity of rotor tip rotates circumferentially and cause NSV.

To inspect the NSV with peak amplitude, the numerical probes as sketched in Fig. 3 are used to acquire the unsteady pressure signal on the blade surface and at the tip clearance. Fig. 11 shows the normalized pressure signal on the blade pressure surface. It is shown that the pressure fluctuation at 88% span larger than those at tip clearance and 78% span. In this study, the peak NSV is found at 88% span (the center of the tornado vortex) near the rotor leading edge pressure surface where the largest pressure oscillation occurs due to the tornado vortex propagation. Note that the pressure signals acquired on the rotor leading edge suction surface also show the peak pressure fluctuations at 88% span in a phase-locked manner similar to those at the pressure surface near leading edge. The high amplitude of unsteady aerodynamic excitation during the NSV as observed in Fig. 11 can induce high cycle fatigue and damage the blade structure.

Fig. 12 shows the predicted frequencies for the normalized pressure signals on the blade suction (top)

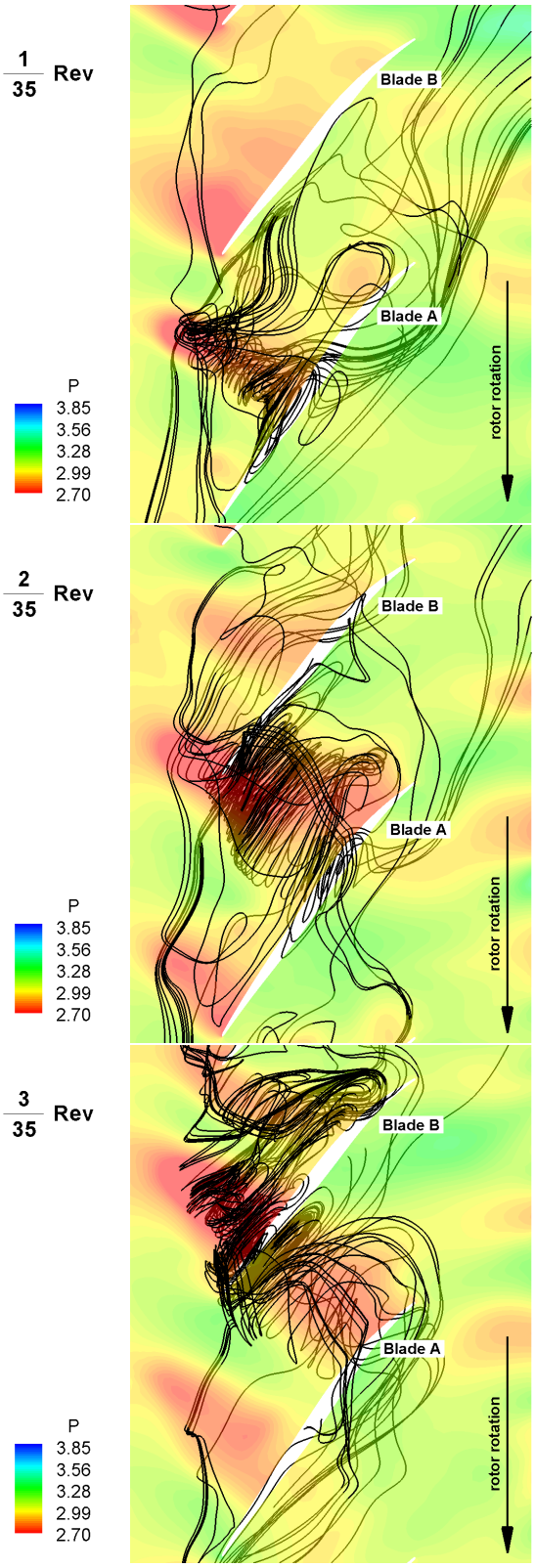

Figure 10: Instantaneous tornado vortex trajectories at 2+1/35, 2+2/35, 2+3/35 Rev colored by the normalized static pressure

and pressure surface (bottom). It is clear that the peak frequency of 2217 Hz is obtained at 88% span near leading edge. The predicted NSV frequency of 2217 Hz is between 10EOL and 11EOL, which is a

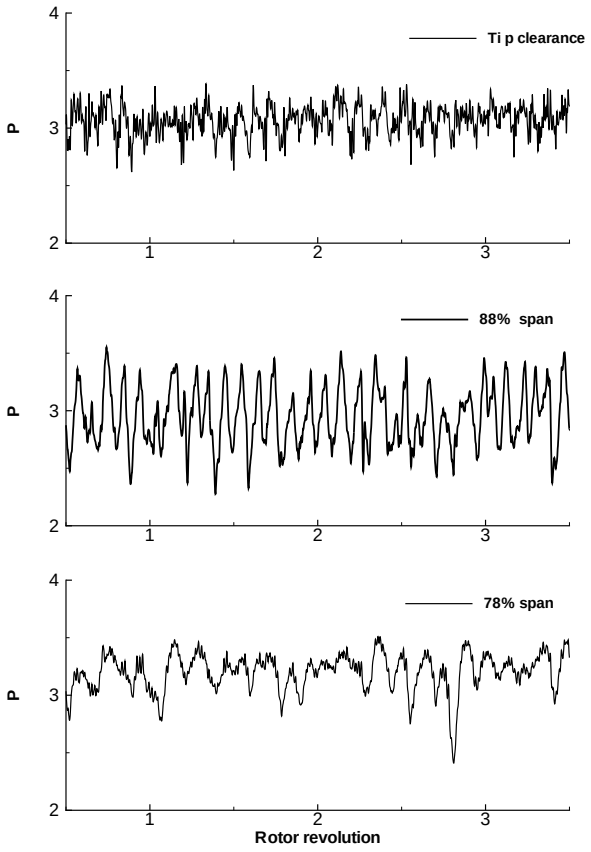

Figure 11: Instantaneous pressure signal on the rotor leading edge pressure surface during the NSV

completely non-synchronous to the engine order and is 14.7% lower than the experiment. The reason is that the DDES tends to predict the rotor stall earlier than the URANS and the NSV can be achieved only at higher mass flow rate, which generates a lower frequency. Note that the base engine order (or 1 EOL) frequency at 12888 rpm is 214.67 Hz. Like the NSV experiment of a high speed axial compressor[1], the present DDES also indicates that the intensity of NSV decreases when the probe is moved away from the rotating instability.

Fig. 13 shows changes in the instantaneous circumferentially mass averaged radial profiles from 2 rotor revolutions including rotor total pressure ratio, mass flux at the rotor outlet, rotor adiabatic efficiency, and relative Mach number at the rotor outlet. The flow above roughly 75% span is very unstable. In particular, there is a large variation of the total pressure ratio around 80% to 90% rotor span, where the NSV of 2217 Hz is observed with peak amplitude in this study.

The total pressure is decreased up to about 80% span, but it dramatically increases roughly above 80% span. The rotor blade loading for pumping work may be too high near the rotor tip, which induces flow separation because of high incidence and further induces the tornado vortex causing NSV. Therefore, redistribution of the blade loading near the rotor tip may be able to mitigate the NSV of the compressor.

Above 80% span the rotor adiabatic efficiency is significantly decreased due to the tornado vortex and the flow blockage. Both the mass flux and relative Mach number at the rotor outlet are lower in the vicinity of the rotor tip during the NSV due to the reversal flow. It is shown that the flow below roughly 70% span is stable during the NSV unlike rotating stall. As aforementioned in the introduction, the experiment for the 10 stage high pressure axial compressor[1] shows a NSV due to a rotating instability with high amplitude vibration on the 1st stage rotor blades above 74% span. In their experiment, the NSV decays from the RI center and eventually disappears below 65% blade span.

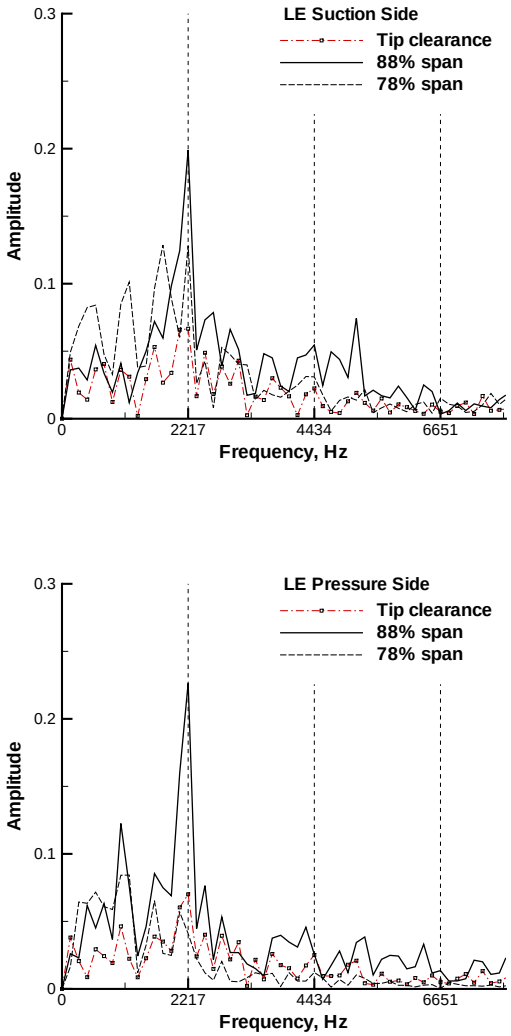

Figure 12: Predicted NSV frequencies for the blade pressure signals acquired at the rotor LE suction (top) and pressure surface (bottom)

7 Conclusion

This paper conducts DDES to study the detailed mechanism of NSV for a high speed axial compressor. The predicted NSV frequency is lower than the measured one, but it still reveals the cause of NSV. It is shown that the tornado vortex formed in the vicinity of rotor tip propagates at the speed of a non-engine order frequency and causes the NSV.

The tornado vortex travels fast on the suction surface of the blade and stays relatively longer at the passage outlet crossing to the next blade leading edge. Such a tornado vortex motion trajectory generates two low pressure regions due to the vortex core positions, one at the leading edge and one at the trailing edge, both are oscillating due to the vortex coming and leaving. These two low pressure regions create a pair of coupling forces that generates a torsion moment causing NSV.

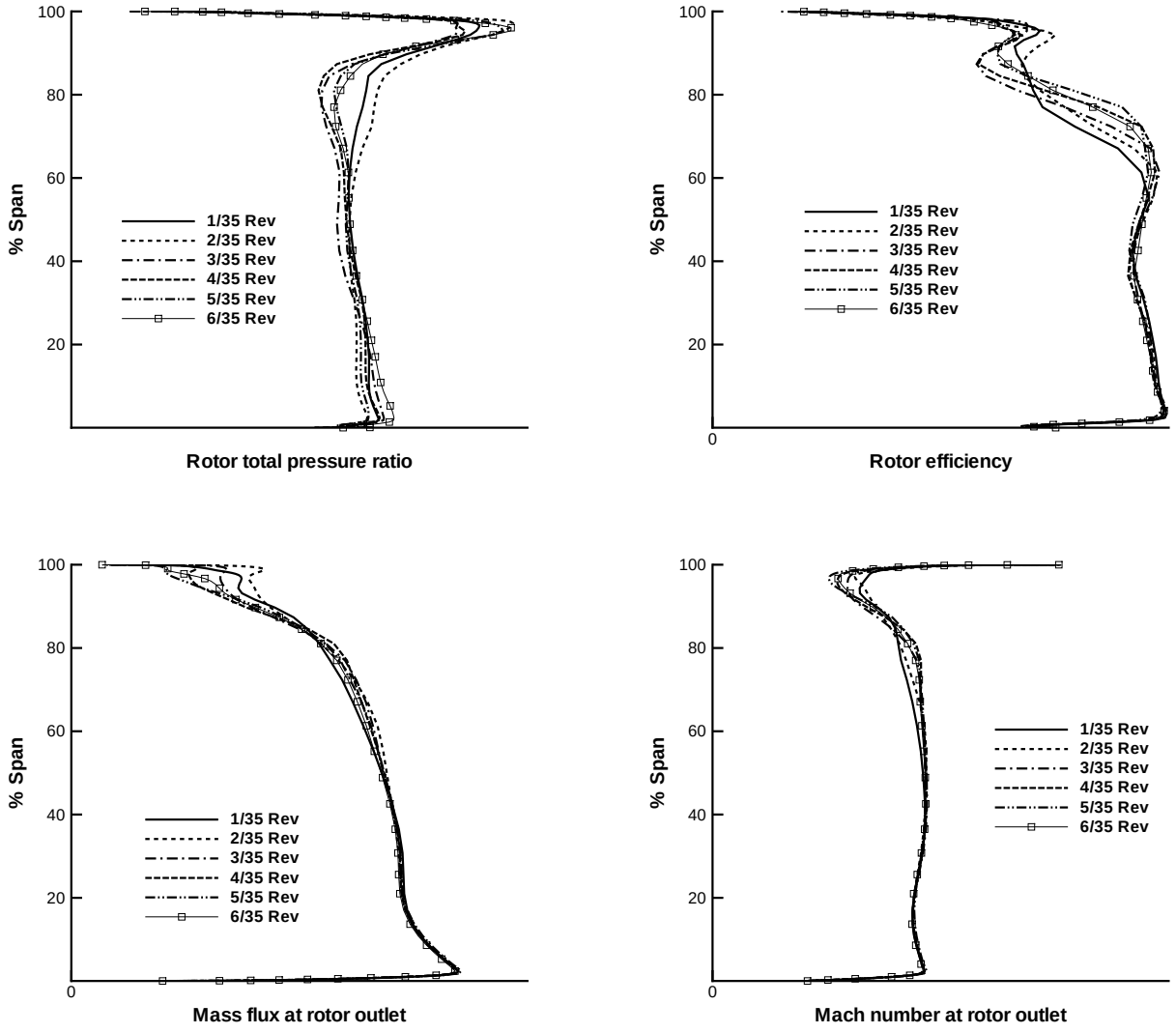

Figure 13: Circumferentially mass averaged radial profiles for the 1st stage rotor; rotor total pressure ratio (top left), rotor adiabatic efficiency (top left), mass flux at rotor outlet (bottom right), rotor outlet relative Mach number (bottom right)

Acknowledgments

We greatly appreciate LC Colmenero and Steve Manwaring at GE Aviation for providing feedback and support. The grants support from AFRL and the industrial partners of GUIde Consortium, 10-AFRL-1024 and 09-GUIDE-1010, are acknowledged. The numerical simulation are conducted at the Center for Computational Sciences at the University of Miami and Air Force Research Lab DoD Supercomputing Resource Centers.

Nomenclature

d	distance from the closest wall
ΔS	Change of entropy, $C_p ln\frac{To}{To_\infty} - Rln\frac{Po}{Po_\infty}$
μ_{DES}	turbulent eddy viscosity determined by DES

ν	kinematic viscosity
$\tilde{\nu}$	working variable of the S-A model related to turbulent eddy viscosity

Abbreviations

BC	Boundary Condition
$CUSP$	Convective Upwind and Splitting Pressure
DES	Detached Eddy Simulation
$DDES$	Delayed Detached Eddy Simulation
IGV	Inlet Guide Vane
NSV	Non-Synchronous Vibration
RI	Rotating Instability
SFV	Separated Flow vibration
$URANS$	Unsteady Reynolds-Averaged Navier-Stokes
$WENO$	Weighted Essentially Non-Oscillatory

References

[1] M. Baumgartner, F. Kameier, and J. Hourmouziadis, "Non-Engine Order Blade Vibration in a High Pressure Compressor." ISABE, Twelfth International Symposium on Airbreathing Engines, Melbourne, Australia, 10-15, 1995.

[2] J. Marz, C. Hah, and W. Neise, "An Experimental and Numerical Investigation Into the Mechanisms of Rotating Instability," *Journal of Turbomachinery*, vol. 124, pp. 367–375, 2002.

[3] R. Mailach, I. Lehmann, and K. Vogeler, "Rotating Instabilites in an Axial Compressor Originating From the Fluctuating Blade Tip Vortex." ASME Paper No. GT-2003-38634, 2003.

[4] R. Kielb, J. Thomas, P. barter, and K. Hall, "Blade Excitation by Aerodynamic Instabilites - A Compressor Blade Study." ASME Paper No. GT-2003-38634, 2003.

[5] H.S. Im, and G.C. Zha, "Effects of Rotor Tip Clearance on Non-Synchronous Blade Vibration for an Axial Compressor." ASME GT2012-68148, 2012.

[6] P.R. Spalart, W.H. Jou, M. Strelets, and S.R. Allmaras, "Comments on the Feasibility of LES for Wings, and on a Hybrid RANS/LES Approach." Advances in DNS/LES, 1st AFOSR Int. Conf. on DNS/LES, Greyden Press, Columbus, H., Aug. 4-8, 1997.

[7] M. Shur, P.R. Spalart, M. Strelets, and A. Travin, "Detached Eddy Simulation of an Airfoil at High Angle of Attack", 4th Int. Symp. Eng. Turb. Modeling and Measurements, Corsica." May 24-26, 1999.

[8] H.S. Im, and G.C. Zha, "Delayed Detached Eddy Simulation of a Stalled Flows Over NACA0012 Airfoil Using Higher Order Schemes." AIAA Paper 2011-1297, Jan. 2011.

[9] H.S. Im, X.Y. Chen, and G.C. Zha, "Detached Eddy Simulation of Stall Inception for a Full Annulus Transonic Rotor," *Journal of Propulsion and Power*, vol. 28 (No. 4), pp. 782–798, doi: 10.2514/1.58970, 2012.

[10] S. Clark, R. Kielb, and K. Hall, "Developing a Reduced-Order Model to Understand Nonsynchronous Vibration (NSV) in Turbomachinery." ASME GT2012-68145, 2012.

[11] G.C. Zha, Y.Q. Shen, and B.Y. Wang, "An Improved Low Diffusion E-CUSP Upwind Scheme ," *Journal of Computer and Fluids*, vol. 48, pp. 214–220, 2011, doi:10.1016/j.compfluid.2011.03.012.

[12] Y.Q. Shen, G.C. Zha, and B.Y. Wang, "Improvement of Stability and Accuracy of Implicit WENO Scheme," *AIAA Journal*, vol. 47, pp. 331–334, DOI:10.2514/1.37697, 2009.

[13] Y.Q. Shen, B.Y. Wang, and G.C. Zha, "Implicit WENO Scheme and High Order Viscous Formulas for Compressible Flows ." AIAA Paper 2007-4431, 2007.

[14] B. Wang, Z. Hu, and G. Zha, "A General Sub-Domain Boundary Mapping Procedure For Structured Grid CFD Parallel Computation," *AIAA Journal of Aerospace Computing, Information, and Communication*, vol. 5, pp. 425–447, 2008.

[15] P.R. Spalart, S. Deck, M. Shur, and K.D. Squires, "A New Version of Detached Eddy Simulation, Resistant to Ambiguous Grid Densities," *Theoritical and Computational Fluid Dynamics*, vol. 20, pp. 181–195, 2006.

[16] P.R. Spalart, and S.R. Allmaras, "A One-equation Turbulence Model for Aerodynamic Flows." AIAA-92-0439, 1992.

[17] H.S. Im, X.Y. Chen, and G.C. Zha, "Simulation of 3D Multistage Axial Compressor Using a Fully Conservative Sliding Boundary Condition." ASME IMECE2011-62049, International Mechanical Engineering Congress & Exposition, Denver, November 2011, 2011.

[18] H.S. Im, and G.C. Zha, "Simulation of Non-Synchronous Blade Vibration of an Axial Compressor Using a Fully Coupled Fluid/Strcuture Interaction." ASME GT2012-68150, 2012.

[19] J. Thomassin, H. Vo, and N. Mureithi, "Blade Tip Clearance Flow and Compressor Nonsynchronous Vibrations: The Jet Core Feedback Theory as the Coupling Mechanism," *Journal of Turbomachinery*, vol. 131, pp. 11013–1–11013–9, 2009.

[20] M. Inoue, M. Kuroumaru, S. Yoshida, and M. Furukawa, "Short and Long Length-Scale Disturbances Leading to Rotating Stall in an Axial Compressor Stage With Different Stator/Rotor Gaps ," *AMSE J. of Turbomach.*, vol. 124, pp. 376–385, 2002, doi:10.1115/1.1458022.